Optimized fluorescent proteins for the rhizosphere-associated bacterium Bacillus mycoides with endophytic and biocontrol agent potential

Yi, Yanglei; Frenzel, Elrike; Spoelder, Jan; Elzenga, J. Theo M.; van Elsas, Jan Dirk; Kuipers, Oscar P.

Published in:
Environmental microbiology reports

DOI:
10.1111/1758-2229.12607

Publication date:
2018

environmental microbiology reports

Environmental Microbiology Reports (2018) **10**(1), 57–74 doi:10.1111/1758-2229.12607

Optimized fluorescent proteins for the rhizosphere-associated bacterium *Bacillus mycoides* with endophytic and biocontrol agent potential

Yanglei Yi,[1†] Elrike Frenzel,[1†] Jan Spoelder,[2] J. Theo M. Elzenga,[2] Jan Dirk van Elsas[3] and Oscar P. Kuipers[1*]

[1]*Department of Molecular Genetics, Groningen Biomolecular Sciences and Biotechnology Institute, University of Groningen, Groningen, The Netherlands.*

[2]*Plant Physiology, Groningen Institute for Evolutionary Life Sciences, University of Groningen, Groningen, The Netherlands.*

[3]*Microbial Ecology, Groningen Institute for Evolutionary Life Sciences, University of Groningen, Groningen, The Netherlands.*

Summary

Tracking of fluorescent protein (FP)-labelled rhizobacteria is a key prerequisite to gain insights into plant-bacteria interaction mechanisms. However, the performance of FPs mostly has to be optimized for the bacterial host and for the environment of intended application. We report on the construction of mutational libraries of the superfolder green fluorescent protein sfGFP and the red fluorescent protein mKate2 in the bacterium *B. mycoides*, which next to its potential as plant-biocontrol agent occasionally enters an endophytic lifestyle. By fluorescence-activated cell sorting and comparison of signal intensities at the colony and single-cell level, the variants sfGFP(SPS6) and mKate (KPS12) with significantly increased brightness were isolated. Their high applicability for plant-bacteria interaction studies was shown by confocal laser scanning microscopy tracking of FP-tagged *B. mycoides* strains after inoculation to Chinese cabbage plants in a hydroponic system. During the process of colonization, strain EC18 rapidly attached to plant roots and formed a multicellular matrix, especially at the branching regions of the root hair, which probably constitute entrance sites to establish an endophytic lifestyle. The universal applicability of the novels FPs was proven by expression from a weak promoter, dual-labelling of *B. mycoides*, and by excellent expression and detectability in additional soil- and rhizosphere-associated *Bacillus* species.

Received 18 August, 2017; accepted 23 November, 2017. *For correspondence. E-mail: o.p.kuipers@rug.nl; Tel. +31 50 363 2093; Fax +31 50 363 2348.

†These authors contributed equally to this work.

Introduction

Fluorescent proteins (FPs) are widely used in living prokaryotic and eukaryotic cells as genetically encoded fluorescent labels to study cell motility, changes in gene activity and protein localization and dynamics (Chudakov *et al.*, 2010; Kremers *et al.*, 2011). After discovery of the first FP, the green fluorescent protein (GFP) of *Aequoria victoria* (Shimomura *et al.*, 1962), cloning of its structural gene paved the way for extensive protein engineering studies (Prasher *et al.*, 1992). These resulted in a plethora of diverse FPs with emission light wavelengths ranging from blue at 448 nm to yellow at 526 nm. Until now, the palette of colour variants for multicolour imaging is constantly expanded (Day and Davidson, 2009). Extensive efforts have also been made to identify and engineer red FPs (RFP) that emit in the yellow-orange to far-red regions of the visible light spectrum (Piatkevich *et al.*, 2010; Shemiakina *et al.*, 2012; Rodriguez *et al.*, 2016). The usage of RFPs is especially advantageous in mammalian cells or plant tissues because these are more transparent to red light (Rizzo *et al.*, 2009). This enables high-contrast imaging due to a low autofluorescence background, as RFPs are highly compatible with existing confocal-microscope lasers and the respective filter sets.

In environmental microbiology, ecophysiology and particularly in plant-microorganism interaction studies, the application of FP markers has recently become a powerful approach for exploring microbial functions *in situ* in natural ecosystems, e.g., the rhizosphere and plant endosphere. Applying biosensor strains for analysing the microbial function in symbiotic or competing communities has led to significant advances in these areas (Larrainzar *et al.*, 2005). However, an on-site and widespread application of FPs in plant ecophysiology is still restricted by the complexity of the rhizosphere and

endosphere environments and matrices. Unlike the laboratory-based *in vitro* systems, rhizosphere samples are usually associated with complex organic and inorganic materials, which show high background levels of autofluorescence when studied with visualization tools like fluorescence microscopy. Moreover, plant roots are able to actively alter the rhizospheric oxygen content and pH (Blossfeld *et al*., 2011), which in turn can affect the brightness of FPs by impeding chromophore maturation (Heim *et al*., 1994; Shu *et al*., 2006), altering the chromophore protonation state (Das *et al*., 2003) or causing misfolding of the FP (Craggs, 2009). Additionally, the functionality of FPs is highly dependent on the bacterial expression host and often needs to be validated or even optimized to fulfil the desired experimental requirements (Hebisch *et al*., 2013). For *in situ* studies using FP-tagged organisms, it is, therefore, of special importance to consider that extrinsic and intrinsic cellular factors impact or modulate the performance of FPs (Shaner *et al*., 2005).

B. mycoides is a chain-forming bacterium, which is associated with the *Bacillus cereus sensu lato* group. This species has a particular asymmetric 'hairy' shape on agar plates. The bundles of filaments resulting from extensive chaining and linkage of cells show either a clockwise or counterclockwise growth pattern (Di Franco *et al*., 2002). *B. mycoides* is ubiquitous and abundant in soils and the rhizosphere of plants, its natural niches (Neher *et al*., 2009; Ambrosini *et al*., 2016). Although *B. mycoides* was occasionally isolated from food cross-contaminated from soil (Samapundo *et al*., 2014), it is widely recognized as a non-pathogenic bacterium (Nakamura and Jackson, 1995). It has a low thermotolerance of 37°C with an optimal growth temperature between 25°C and 30°C (Guinebretière *et al*., 2008). Various *B. mycoides* strains isolated from the rhizosphere show plant growth-promoting effects on several crops. It was for instance shown that the *B. mycoides* isolate S4 promotes phosphorous solubilisation and iron release by its siderophore production activity, which increases the photosynthesis and chlorophyll content of the runner bean *Phaseolus coccineus* L. (Stefan *et al*., 2013). Moreover, elicitation of an induced systematic resistance (ISR) by *Bacillus* strains led to a significant reduction in the severity or incidence rates of various diseases on a diversity of plant hosts (Kloepper *et al*., 2004). Elicitation of ISR on sugar-beet was found to be associated with increased peroxidase activity coupled to an enhanced production of chitinase by the *B. mycoides* strain BmJ (Bargabus *et al*., 2002; Bargabus *et al*., 2004). This strain was furthermore able to control anthracnose of cucurbits through the induction of systemic acquired resistance (SAR) (Neher *et al*., 2009). The biocontrol potential of *B. mycoides* against the plant pathogens *Sclerotinia sclerotiorum* or *Botrytis cinerea* is based on the bacterial production of antimicrobial products such as bacillomycin D, fengycin, zwittermicin A or volatiles (Guetsky *et al*., 2002; Athukorala *et al*., 2009).

We isolated *B. mycoides* strains from the endosphere of healthy potato plants (Yi *et al*., 2017), which indicates that the interaction could be commensal or mutualistic. However, the ecological relationship between different *B. mycoides* strains and plants has not been exhaustively studied. The observation of various stages of the colonization processes is critical to understand the physiological and molecular mechanisms of bacteria-plant interaction. Although there are many fluorescent tools available for low-GC Gram-positive spore formers, they are not optimized for use in endophytic *B. mycoides*. The lack of optimized fluorescent proteins to label this rhizobacterium for tracking and visualizing its development *in planta* or in hydroponic culture systems, and for labelling of promoters to analyse factors that contribute to its endophytic lifestyle is currently a bottleneck and necessitates further tool development.

In this study, we applied a random mutagenesis approach to generate mutational libraries of the green fluorescent protein sfGFP and the red fluorescent protein mKate2. After *in vivo* isolation of single mutants by fluorescence-activated cell sorting (FACS) and screening of fluorescence intensities during *B. mycoides* colony development by stereo fluorescence microscopy, three brightly expressed candidates for each FP were obtained. Intriguingly, variants selected under pH shifted conditions showed the highest improvement in fluorescence signal intensity. We further demonstrate that these FP variants are suitable for *B. mycoides-in planta* localization studies with the advantage of showing an improved background signal-to-noise ratio. The universal applicability of the novels FPs was further proven by their detectability even when expressed from a weak promoter in *B. mycoides* and by excellent expression and detectability in additional soil- and rhizosphere-associated *Bacillus* species. The successful double-labelling and dual-colour imaging of *B. mycoides* indicates that the improved FPs reported here can be further applied for advanced molecular genetic studies, such as gene expression and protein localization in *B. mycoides*.

Results and discussion

Construction of GFP and RFP libraries and isolation of bright variants by B. mycoides *cell sorting*

FPs are indispensable tools for molecular biology and microbial ecology. However, FPs are not equally well expressed in different bacterial species, presumably due to the codon-usage bias which affects the translation,

folding and maturation efficiency of the proteins. Previous studies proved that different GFP variants display strongly variable fluorescence intensities in low-GC Gram-positive organisms (Overkamp *et al*., 2013).

Our preliminary experiments showed that sfGFP(Sp), a robust, fast-folding and fast-maturing 'superfolder' GFP (Pedelacq *et al*., 2006; Overkamp *et al*., 2013) was functionally expressed in *B. mycoides*. However, the signal was too weak for studying bacteria-plant interactions and cell tracking when sfGFP(Sp) expression was driven by weak promoters (data not shown). To track different bacterial strains at the same time, or to simultaneously follow distinct promoter activities within one cell, it would be desirable that multiple fluorescent markers are well expressed and detectable in the same target organism. Since mKate2 has a fluorescence spectrum that substantially differs from GFP, with an excitation maximum of 588 nm and an emission maximum of 633 nm (Shemiakina *et al*., 2012), it is highly suitable for co-labelling experiments with GFP. However, initial benchmarking experiments with the red fluorescent protein variants mCherry and mKate2 cloned on multicopy plasmids revealed that the signal intensity of mKate2 was very low and close to the level of autofluorescence of *B. mycoides* cells. Moreover, the expression of mCherry could neither be detected by flow cytometry (FC) nor by fluorescence microscopy (data not shown). This is in line with the observation that mKate2 was better suited for promoter labelling studies than mCherry in the closely related species *B. cereus* (Eijlander and Kuipers, 2013).

By applying a random mutagenesis approach, we obtained a sfGFP library that was cloned into the replicative *E.coli-Bacillus* shuttle plasmid pNW33N, resulting in a total of 115,000 *E.coli* TOP10 clones. The plasmids carrying the mutated *sfGFP(Sp)* gene were isolated and transformed into *B. mycoides* EC18 by electroporation, resulting in a library size of 44 000 clones with a mutational frequency of one to four nucleotides per *sfGFP(Sp)* gene. However, mKate2 showed no fluorescence when being expressed under the control of the same *pta* promoter as sfGFP (data not shown). As a result, the mKate2 mutation library was constructed with the replicative plasmid pAD43-25, which carries the comparably stronger *upp* promoter. The plasmid library was transformed into *E.coli* TOP10, thereby yielding a size of 115 200 colonies. The transformation of the library into *B. mycoides* EC18 resulted in a 43 820 clone-sized library with a mutation rate of one to three nucleotides per *mKate2* gene.

To isolate the brightest sfGFP(Sp) and mKate2 mutants, the *B. mycoides* libraries were grown planktonically until the exponential growth phase was reached. We considered that the bacteria encounter environments with different pH during the establishment of the endophytic lifestyle, since cabbage-related plants such as *Arabodopsis thaliana* induce a soil acidification in the rhizosphere region (for a recent publication, see Barbez *et al*., 2017). Therefore, the *B. mycoides* libraries were grown in three groups with different pH conditions: pH 6.0, pH 7.0 and pH shift condition. For the latter, brightest cells were first enriched at pH 6.0, and then subcultured at pH 7.0 followed by a second round of FACS enrichment. As shown in the Supporting Information Fig. S1, around 0.3% of the mildly sonicated cell population was sorted after a first FACS enrichment step from all pH conditions. After spreading and incubation at 30°C on LB-Cm4 agar, 20 of the brightest colonies were selected by visual appearance with a Olympus MVX10 macro zoom fluorescence microscope (Supporting Information Fig. S1). To obtain pure colonies arising from single clones, the 20 preselected colonies from each condition were restreaked twice on LB-Cm4. After quantification of signal intensities and the amplitude of fluorescence signals at the single-cell level from exponential phase cultures by FC, we selected three of the best performing GFP and RFP variants with high brightness and small fluorescence signal deviations for further analyses.

Improvement of GFP signal intensities

The mean fluorescence intensity (MFI) of the sfGFP variants selected under pH 6.0, pH 7.0 and pH shift conditions (termed S618, S709 and SPS6) was measured by FC. As shown in Fig. 1A, the MFI of all selected sfGFP variants was increased by at least 50% in comparison to the original sfGFP reporter in *B. mycoides*. The variant selected under pH shift conditions, sfGFP(SPS6), exhibited the strongest mean fluorescence signal. Signal intensities of single cells stemming from a colony grown on solid medium was examined by fluorescence microscopy (Fig. 1B). In general, the differences in the average fluorescence levels analysed from microscopy images correlated well with the results obtained by FC. The highest improvement with regard to the mean brightness level was observed for the optimized sfGFP(SPS6) protein when compared to the original sfGFP(Sp) protein.

Although the signal intensity of all sfGFP variants was not evenly distributed within single cells, obvious differences in the mean brightness levels between the optimized and the original sfGFP were observed, clearly showing an improved detectability by visualization methods (Fig. 2A and B). Variation of the signals could be related to an uneven distribution of FP proteins and/or differences in the plasmid copy numbers in the daughter cells, as it was previously discussed for the closely related bacterium *B. cereus* (Eijlander and Kuipers,

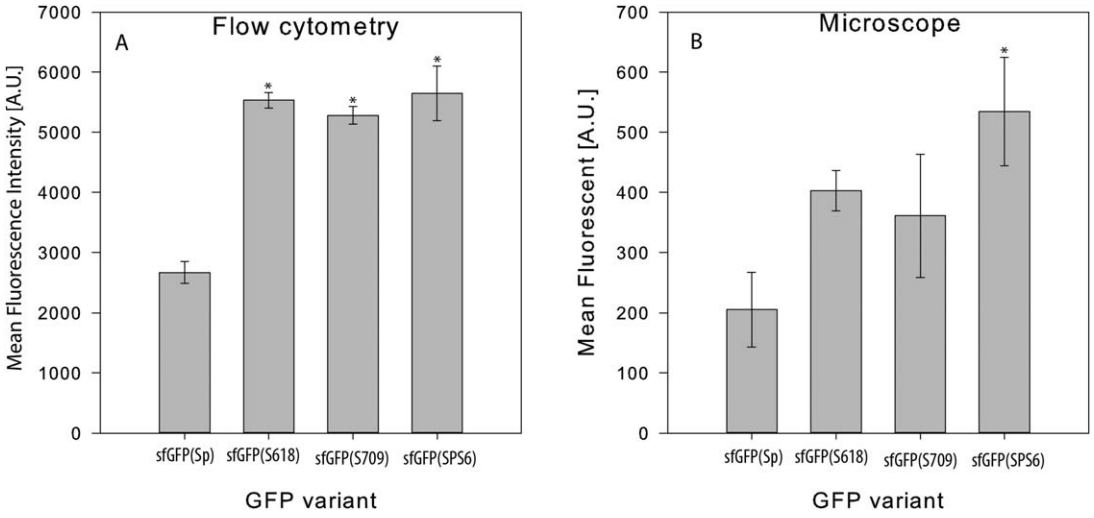

Fig. 1. Fluorescence quantification of sfGFP variants in *B. mycoides*.
A. *B. mycoides* EC18 carrying pNW33N-Ppta-3TER plasmids with the respective fluorescent protein variants were grown overnight in LB and subjected to analysis by FC.
B. Single-cell fluorescence was measured with fluorescence microscopy. The fluorescence intensities are normalized for background fluorescence and cell area (see Material and Methods). Mean fluorescence was calculated from at least 500 cells. Error bars indicate the standard errors of the means obtained from three independent biological and technical replicates. Asterisks denote significant differences between the mean fluorescence intensity of sfGFP and the respective mutant variants ($p < 0.05$).

2013). However, with a few exceptions, the mechanism of cell division and separation (Di Franco *et al*., 2000; Turchi *et al*., 2012) and the possibility that the extensive cell chaining might be connected to multicellular cooperation (Shapiro, 1998), such as the exchange of DNA, nutrients or signals between the *B. mycoides* cells, has not been studied so far. We thus tested the possibility that the constitutive expression of the FPs poses a metabolic burden to the cells and that separating daughter cells might undergo a loss of the replicative plasmid. Comparison of the growth behaviour between *B. mycoides* wild type cells and cells carrying the FP expression plasmids did not reveal any growth retardation or growth defects from early logarithmic to the late stationary phase (Supporting Information Fig. S2A). In addition, fluorescence imaging of complex *B. mycoides* colonies showed that the expression of sfGFP generally did not affect the development of colonies (Fig. 2B). Due to the compactness and multilayered rhizoid growth, however, the difference in brightness between the optimized sfGFP and the original sfGFP(Sp) variants was not as apparent as compared to the measurements of cells grown under planktonic conditions (Fig. 2B). Tracing the plasmid presence and inheritance without antibiotic pressure by sequential propagation over several days (approximately 150 generations) showed no indication of significant plasmid loss (Fig. S2B). This indicates that the plasmid itself is stably inherited and that the reason for signal intensity variation between single cells is more complex and needs to be addressed in greater detail in a separate study.

Improvement of RFP signal intensities

Determination of the MFI of the *in vivo* selected RFP variants revealed that the signal intensities of the mutants K603 and K713 selected under pH 6.0 and pH 7.0 conditions was increased 7- and 6-fold in comparison to the original mKate2 protein (Piatkevich *et al*., 2010) respectively, while mKate2(KPS12), which was selected under pH shift conditions, showed a 10-fold improvement of fluorescence (Fig. 3A). This was further corroborated by the quantification of fluorescence signals emitted from single cells by fluorescence microscopy showing that KPS12 was the best performing mKate2 variant in *B. mycoides* (Fig. 3B). Cells carrying the original mKate2 emitted a very weak fluorescence signal, which was barely above the autofluorescence of *B. mycoides* cells at 528–553 nm excitation. In contrast, K603, K713 and KPS12 showed a significant improvement of fluorescence signal emission (Fig. 4A). Colony imaging revealed that the signal-to-noise ratio was significantly improved for all three variants as compared to mKate2, resulting in clearly detectable colonies on solid growth media. Moreover, in the complex *B. mycoides* colonies, in which cells are less well aerated than in shaken planktonic cultures, KPS12 still gave the highest signals among all examined variants (Fig. 4B).

As observed for the GFP variants, cells showed a variation in the intensity of fluorescence signals when expressing the RFP proteins, which was not caused by growth retardation effects or by a loss of the replicative plasmid encoding the RFP (Supporting Information

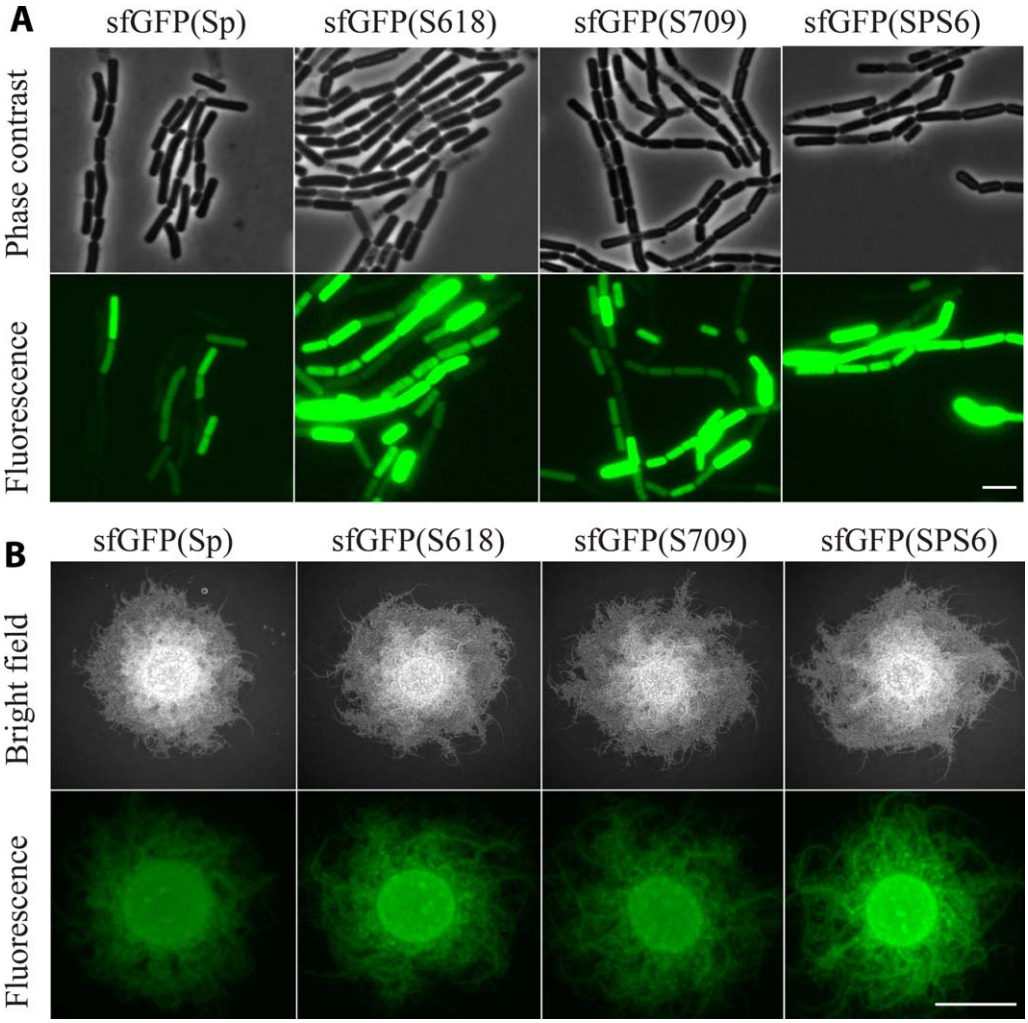

Fig. 2. A. Visualization of sfGFP variant expression in planktonically grown, exponential-state cells of *B. mycoides* by fluorescence microscopy. For comparison of the sfGFP fluorescence intensities, the same imaging conditions were applied (ex: 465–495 nm, em: 515–555 nm; exposure: 0.15 s with 32% excitation xenon light (300 W); 100× phase-contrast objective). The white bar represents 5 μm.
B. Comparison of fluorescence signal intensities of sfGFP variants in *B. mycoides* colonies. LB-Cm4 plates were spot-inoculated with equal amounts of *B.mycoides* cells and incubated for 18 h at 30°C. Images were acquired with a microscope using the same imaging conditions (ex: 460/480 nm, em: 495/540 nm, 50% of excitation light, exposure time: 100 ms). The white scale bar represents 0.5 cm. Representative images from three independent biological replicates are shown.

Fig. S2A and B).The mechanism causing these phenotypic differences thus needs to be addressed in a separate study.

Co-expression of optimized GFP and RFP variants in B. mycoides

Based on the results obtained from protein optimization, we next tested the suitability of the best performing variants for dual-labelling and simultaneous visualization in the *B. mycoides* background. To additionally address the question whether the signal variation could be reduced, we first integrated the sfGFP(SPS6) gene driven by the constitutive P_{pta} promoter into the chromosome of *B. mycoides* EC18 at the α-amylase gene locus. In a next step, the pAD-mKate(KPS12) plasmid was transformed into the single-copy reporter strain to obtain the co-expression strain. The GFP and RFP signals were simultaneously detectable by FC and by fluorescence microscopy and were clearly distinguishable from each other under the given differential excitation and detection conditions, showing that a cross-talk caused by a spectral overlap between the FPs is negligible (Fig. 5). This indicates that neither the excitation nor the emission spectra are significantly changed from the original protein variants, which have been previously shown to be compatible in multicolour imaging studies in *Streptococcus pneumonia* (Kjos *et al*., 2015). To our knowledge, this is the first report of a successful dual-FP-labelling approach in bacilli of the *B. cereus sensu lato* group.

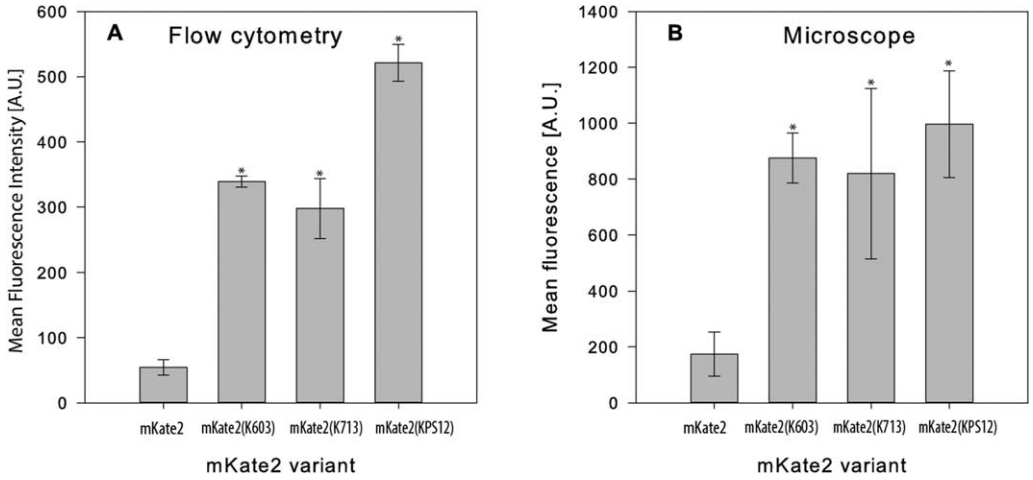

Fig. 3. Fluorescence quantification of mKate2 variants in *B. mycoides*.
A. *B. mycoides* EC18 carrying pAD43-25 plasmid derivatives with the respective fluorescent protein variants were grown overnight in LB and subjected to analysis by FC.
B. Single-cell fluorescence was measured by fluorescence microscopy. Fluorescence intensities are normalized for background fluorescence and cell area and the mean fluorescence was calculated from at least 500 cells. Error bars indicate the standard errors of the means ($n = 3$). Asterisks denote significant differences between the mean fluorescence intensity of mKate2 and the respective mutant variants ($p < 0.05$).

Notably, the GFP signal intensity distribution was more homogeneous within the cells due to the presence of a chromosomally integrated single copy of the *gfp* gene (Fig. 5D). This in turn strongly indicates that the differences in plasmids copy numbers among daughter cells within a colony substantially impact the signal amplitude per cell.

FP expression from a mannose-inducible promoter

For plant-interaction studies, it would further be desirable to confirm the expression of the optimized FP variants when driven by weak or condition-dependent promoters. This is currently hampered by the lack of systematically characterized promoter regions in *B. mycoides*. We initially recognized that a mannose-inducible promoter (P*man*) from *B. subtilis* (Altenbuchner, 2016) is 'leaky' in *B. mycoides*, thereby conferring a basal, low level of FP expression. To compare the performance of the optimized and original FPs under the control of P*man*, fusions were constructed based on the replicative plasmid pAD (Table 1) and transformed into *B. mycoides* EC18. FC measurements revealed that both optimized variants sfGFP(SPS6) and mKate(KPS12) were significantly better detectable than the parental FP versions (Supporting Information Fig. S3). The MFI stemming from the optimized variants increased with increasing mannose concentrations, whereas no significant MFI increase could be observed for the original proteins. This shows that that the improved variants are better suited for the detection when fused to weak promoters, because the parental FPs are only expressed at levels close to the autofluorescence of *B. mycoides* cells under these conditions.

Expression of novel FPs in other rhizosphere-associated Bacillus *strains*

Although this study mainly focused on the development of optimized FP variants to allow the tracing of root-associated and endophytic *B. mycoides* strains, we next tested the performance of the improved FPs in additional *Bacillus* species that mainly thrive in the soil. The sfGFP variant SPS6 was transformed into *B. cereus* ATCC 10987, *B. subtilis* HS3 and *B. amyloliquefaciens* HS9. The strains HS3 and HS9 were isolated from grass rhizosphere and are potentially PGP-promoting (unpublished data). In comparison to the original sfGFP(Sp) protein, sfGFP(SPS6) showed a 3- to 5-fold, significantly improved fluorescence intensity in all three strains, thereby facilitating their detection by fluorescence microscopy (Fig. 6A–C). The improvement of brightness of mKate(KPS12) is shown in Fig. 6D–F. While expression of the original mKate2 variant was barely measurable in *B. cereus* ATCC 10987, as stated earlier (Eijlander and Kuipers, 2013), mKate(KSP12) showed a fivefold improved brightness and was detectable by both fluorescence microscope and FC (Fig. 6D). A significant increase in brightness was also observed in the rhizosphere-derived *B. subtilis* HS3 and *B. amyloliquefaciens* HS9 hosts (Fig 6E and F). Altogether, the improved variants were well expressed in the species tested and considerably facilitated the detection of *Bacillus* strains by live-cell imaging methods.

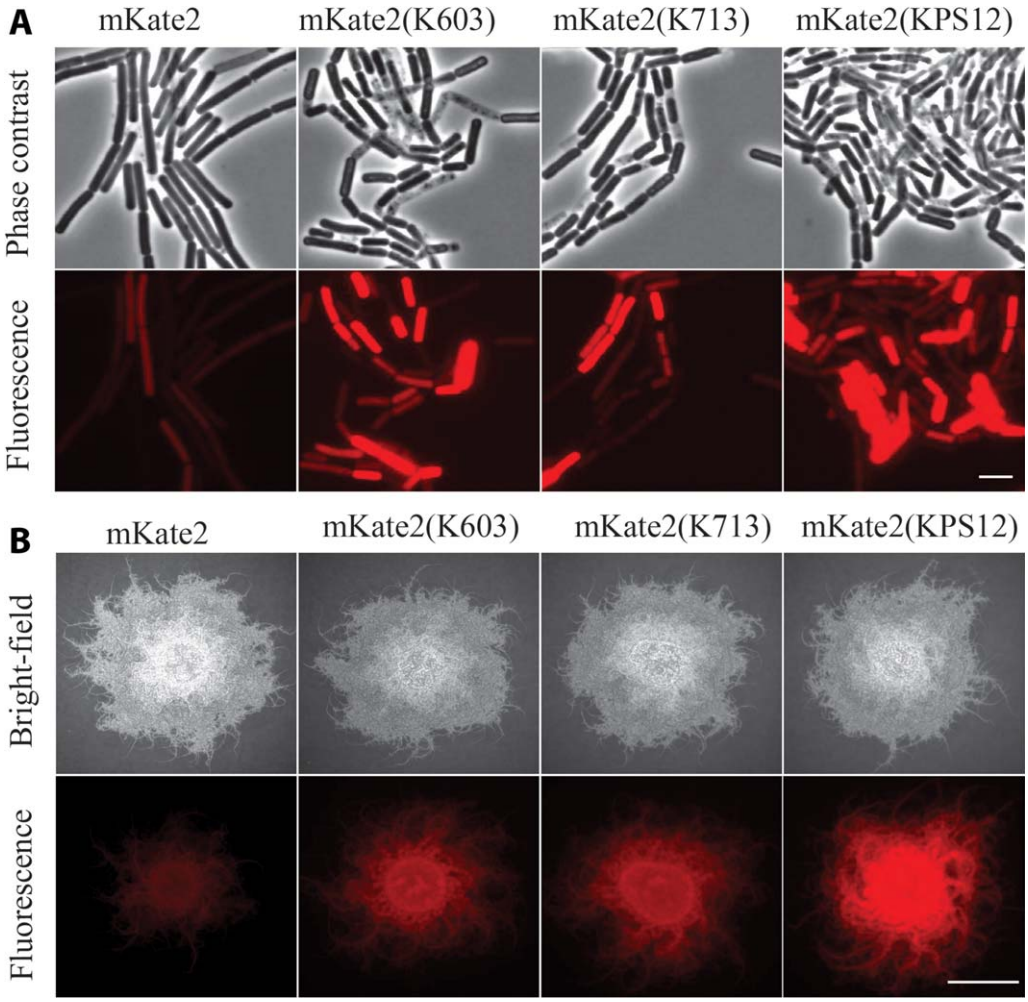

Fig. 4. A. Visualization of mKate2 variant expression in planktonically grown, exponential-state cells of *B. mycoides* by fluorescence microscopy. For comparison of the mKate2 fluorescence intensities, the same imaging conditions were applied (ex: 528/553 nm, em: 590/650 nm; exposure: 0.45 s with 50% excitation xenon light (300 W); 100× phase-contrast objective). The white bar represents 5 μm.
B. Comparison of fluorescence signal intensities of mKate2 variants in *B. mycoides* colonies. LB-Cm4 plates were spot-inoculated with equal amounts of sporulated *B. mycoides* cells and incubated for 18 h at 30°C. Images were acquired with a microscope using the same imaging conditions (ex: 545/580 nm, em: 610 nm, 100% of excitation light, exposure time: 3.5 s). The white scale bar represents 0.5 cm. Representative images from three independent biological replicates are shown.

In situ *performance of improved FPs to localize* B. mycoides *during establishment of an endophytic lifestyle*

In the rhizosphere, bacteria-plant interactions play an important role in maintaining plant health. The possibility of visualizing these interactions *in situ* is a key step for understanding the ecophysiology and basic biology underlying the beneficial processes (Larrainzar *et al*., 2005). Germaine *et al*. (2004) studied the endophytic behaviour of three *Pseudomonas* species by tracing the GFP-labelled cells during colonization of poplar trees. Bloemberg *et al*. (2000) labelled *P. fluorescens* with the enhanced cyan FP, enhanced green FP, enhanced yellow FP and the DsRed RFP reporter protein. After inoculation of tomato plant seedlings, mixed microcolonies as well as single populations could be simultaneously visualized, which revealed a dynamic behaviour of localizing to sites on the roots and in the root/soil interface.

To finally demonstrate the applicability of the *in vivo* selected GFP and RFP variants for *in planta* studies, the endophytic *B. mycoides* isolate EC18 expressing the different FP proteins from constitutive promoters was inoculated on Chinese cabbage (*Brassica rapa*) roots in a hydroponic system. At day 2 and day 3 after inoculation, roots were sampled and analysed concerning fluorescence signals and *in planta* localization of *B. mycoides* by confocal microscopy. For GFP, both the original sfGFP(Sp) (Fig. 7A) and the variant sfGFP(SPS6) (Fig. 7B and C) provided a well-detectable fluorescence signal at very low excitation strength, which prevented the occurrence of an autofluorescence background from

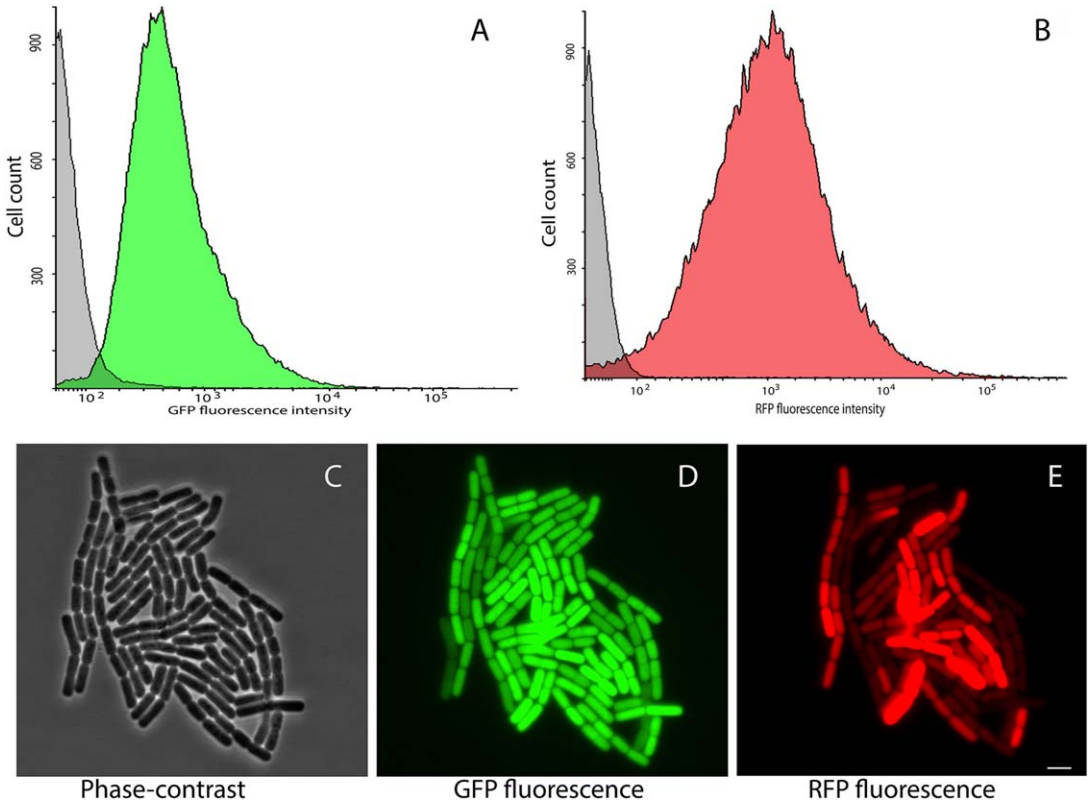

Fig. 5. Co-expression of optimized FPs in *B. mycoides* EC18. The strain was double-labelled by chromosomal integration of a single copy of sfGFP(SPS6) into the *amyE* locus and electroporation of the replicative plasmid pAD-mKate2(KPS12) into the reporter strain.
A and B. FC measurements of GFP and RFP channels.
C–E. Microscopic observation from phase-contrast, GFP (ex: 465–495 nm, em: 515–555 nm; exposure: 2.62 s with 32% excitation xenon light), and RFP (ex: 528/553 nm, em: 590/650 nm; exposure: 0.637 s with 50% excitation xenon light) channels.

the root cells. In contrast to sfGFP(Sp), cells tagged with the SPS6 mutant were more readily detectable; indicating that the higher brightness observed in fluorescence microscopy and FC experiments is also advantageous for confocal microscopy applications. At 2 days post inoculation (DPI), *B. mycoides* initiated the attachment to the epidermis of the primary roots (Fig. 7B). After 3 DPI, the bacteria started to aggregate as microcolonies on the surface, especially at the emerging site of root hairs. Additionally, a few chaining cells that translocated into the endosphere were observed (Fig. 7C). Interestingly, junctions of primary and lateral roots seem to be a preferred niche for microcolony establishment of *B. amyloliquefaciens* FZB42 (Fan *et al*., 2011), which might indicate that these are preferred sites for feeding on nutrients or endophytic entry into the plant.

Similar bacteria-plant interaction patterns were observed when *B. mycoides* was labelled with the red spectrum reporter protein variant mKate2 (Fig. 7D) and mKate2(KPS12) (Fig. 7E and F). Due to the inherently low fluorescence intensity of the original mKate2 protein during expression in *B. mycoides*, the fluorescent signal is very weak and can hardly be detected (Fig. 7D). Enhancement of the excitation power and digit gain settings also deteriorated the signal-to-noise ratio and thus induced a high autofluorescence background of the plant tissue (data not shown). In comparison, the enhanced fluorescence intensity of the mutant KPS12 allowed the detection of *B. mycoides* above the autofluorescence of the root hairs without extensive adjustment of the excitation parameters. Two days after inoculation, *B. mycoides* cells were attached to root hair cells (Fig. 7E). These interactions were shown to play a key role in the endophytic colonization of olive plant roots by *Pseudomonas* species (Prieto *et al*., 2011). Three days after inoculation, a higher number of cells were aggregated on the root epidermis and some cells were growing in the endosphere of the root hair as well as in the main root. A massive amount of *B. mycoides* cells colonized the elongation region of the root hair, which might represent an entrance point for *B. mycoides* to establish an endophytic lifestyle (Fig. 7F). Similarly, Ji and colleagues (2008) observed that the endophytic *B. subtilis* strain Lu144 enters into mulberry seedlings through the cracks formed at the lateral root junctions and the zone of differentiation and elongation. We speculate that the junctions of root hairs and main roots are the preferred and specific

Table 1. Strains, plasmids and primers used in this study.

Strains	Relevant characteristic	Reference
B. mycoides EC18	Wild type. Isolated from potato endosphere.	Yi and colleagues (2017)
B. subtilis HS3	Wild type. Isolated from grass rhizosphere.	Z. Li. (Unpublished)
B. amyloliqefaciens HS9	Wild type. Isolated from grass rhizosphere.	Z. Li. (Unpublished)
B. cereus ATCC 10987	*B. cereus* type strain	Rasko and colleagues (2004)
E. coli TOP10	F- mcrA △(mrr-hsdRMS-mcrBC) φ80*lac*Z △M15 △*lac*X74 *rec*A1 *araD*139 △ (*ara-leu*)7697 *gal*U *gal*K *rps*L *end*A1 *nup*G	Laboratory stock University of Groningen
Plasmids		
pKB01-sfGFP(Sp)	*E.coli-Streptococcus* shuttle vector encoding super folder GFP codon-optimized for *Streptococcus pneumoniae*; Ap^R; Tet^R	(Overkamp *et al.*, 2013)
pNW-P_{pta}-3TER	*E. coli-Bacillus spp.* shuttle vector for FP library construction. Constitutive P_{pta} promoter from *Parageobacillus thermoglucosidasius* DSM 2542 and three-fold transcriptional terminator derived from pKB01; replicates in *Bacillus* strains with pBC1 origin Cm^R	(Frenzel *et al.* 2017; submitted manuscript)
pAD651	*E. coli-Bacillus spp.* shuttle vector encoding mKate2; replicates in *Bacillus* strains with pTA1060 origin; Ap^R; Cm^R	(Eijlander and Kuipers, 2013)
pAD43-25	*E. coli-Bacillus spp.* shuttle vector for FP library construction.; constitutive P_{upp} promoter from *B. cereus* UW85; replicates in *Bacillus* strains with pTA1060 origin Ap^R; Cm^R	(Dunn and Handelsman, 1999)
pNW-sfGFP(S618)	Derivative of pNW-P_{pta}-3TER encoding sfGFP(S618) for optimized expression in *B. mycoides*	This study
pNW-sfGFP(S709)	Derivative of pNW-P_{pta}-3TER encoding sfGFP(S709) for optimized expression in *B. mycoides*	This study
pNW-sfGFP(SPS6)	Derivative of pNW-P_{pta}-3TER encoding sfGFP(SPS6) for optimized expression in *B. mycoides*	This study
pAD-mKate(K603)	Derivative of pAD43-25 encoding mKate(K603) for optimized expression in *B. mycoides*	This study
pAD-mKate(K713)	Derivative of pAD43-25 encoding mKate(K713) for optimized expression in *B. mycoides*	This study
pAD-mKate(KPS12)	Derivative of pAD43-25 encoding mKate(KPS12) for optimized expression in *B. mycoides*	This study
PYB_amyGFP	Derivative of PATΔS28. Replicative in *E. coli* and conditionally replicative in *Bacillus species*. Expression of the sfGFP(SPS6) gene is driven by the constitutive P_{pta} promoter from *P. thermoglucosidasius* DSM 2542; $Spec^R$.	This study
pAD-KPS12-P*man*	Derivative of pAD-mKate(KPS12). The *upp* promoter was replaced by mannose inducible promoter.	This study
pAD-mKate2-P*man*	Derivative of pAD-mKate2. The *upp* promoter was replaced by mannose inducible promoter.	This study
pAD-sfGFP(Sp)-P*man*	Derivative of pAD-KPS12-P*man*. The RFP gene was replaced by *gfp*(Sp)	This study
pAD-SPS6-P*man*	Derivative of pAD-KPS12-P*man*. The RFP gene was replaced by *gfp*(SPS6)	This study
Primers		
pKBO1derMut_F	TCCTCTAGAACTAATAAGGAGGACAAACATG (XbaI)	(Frenzel *et al.*, 2017, submitted manuscript)
pKBO1derMut_R	CCTGCATGCCCTTGACTAGTGCTCATTATTA (SphI)	(Frenzel *et al.*, 2017, submitted manuscript)
pNW33N_for	TCGGGATTCGTTTTACTTTCC	(Frenzel *et al.*, 2017, submitted manuscript)
pNW33N_rev	CAATTTCACACAGGAAACAGC	(Frenzel *et al.*, 2017, submitted manuscript)
mKate2Mut_F	GACTCTAGAGGAAAATTAATGTCAGAACTT (XbaI)	This study
mKate2Mut_R	ACTGCATGCCTACTCAAGCTTTTATTATTA (SphI)	This study
pAD_for	ATTGAAGAAGACTGCCGAGACT	This study
pAD_rev	CGAAGCTCGGCGGATTTGTC	This study
amyF	GAGCGGTACCTCATTTTGACGGAACGGATTG (KpnI)	This study
amyR	GAGCGAGCTCTTCATCACCAATTTACCGCTG (SacI)	This study
PmanF	GAGCGAATTCGCAGGGATTATTCCTTGCTTT (EcoRI)	This study
PmanR	GAGCTCTAGATGTCTCAACTGTATACCGAAATC (XbaI)	This study

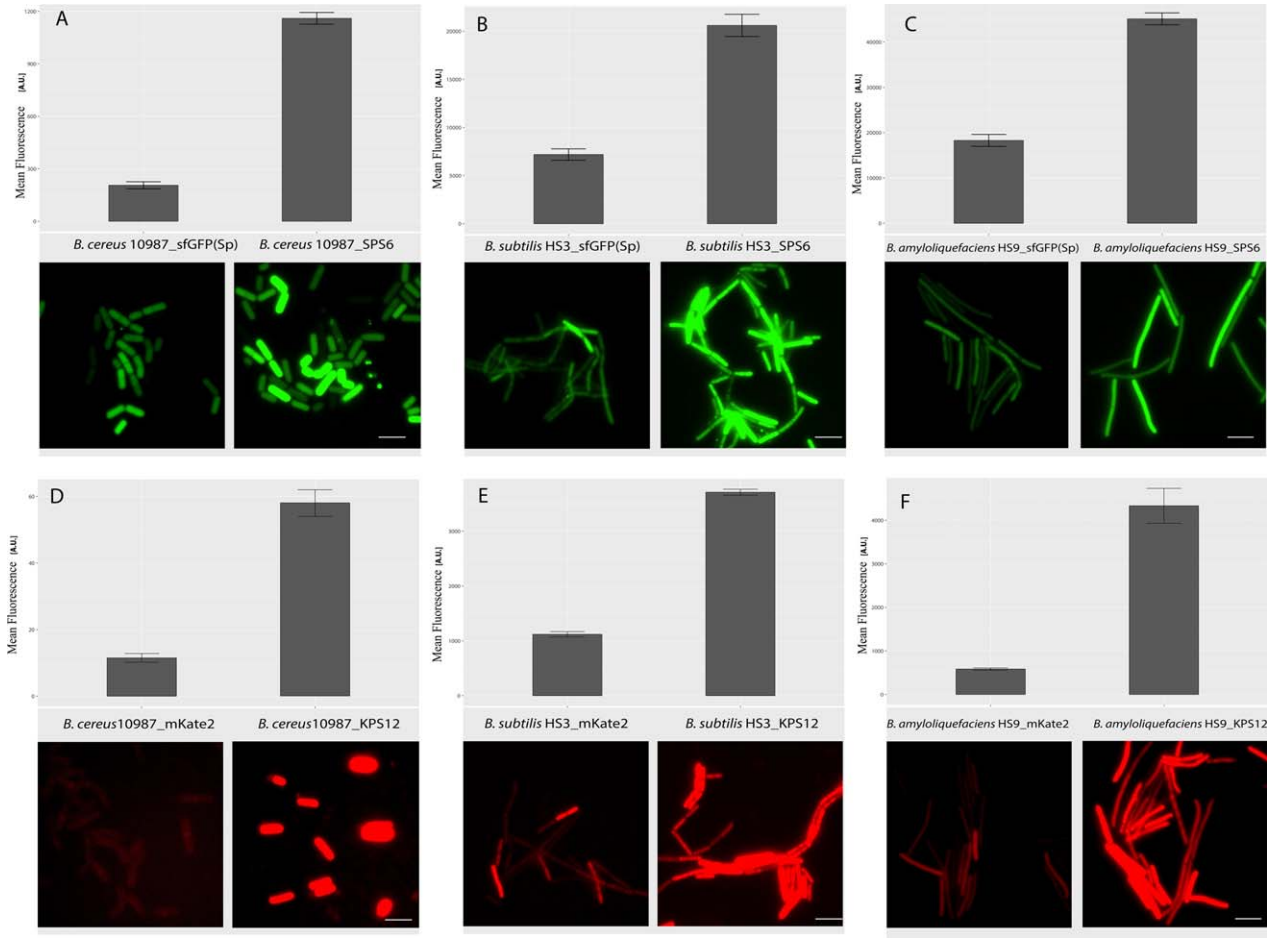

Fig. 6. Comparison of the performance of the original and optimized FP variants in additional soil and rhizosphere-derived *Bacillus* species. The sfGFP imaging conditions were the same for each strain (ex: 465–495 nm, em: 515–555 nm with 32% xenon light excitation), but different exposure times were applied. Exposure time (A) *B. cereus* ATCC 10987 is 0.4 s; (B) *B. subtilis* HS3 is 0.085 s and (C) *B. amyloliquefaciens* HS9 is 0.050 s. The imaging conditions for mKate2 variants were the same for each strain (ex: 528/553 nm, em: 590/650 nm with 50% excitation xenon light), but different exposure time were applied. The exposure time for: (A) *B. cereus* ATCC 10987 is 30 s; (B) *B. subtilis* HS3 is 0.33 s and (C) *B. amyloliquefaciens* HS9 is 3.75 s. Representative images are shown. The white bar represents 5 μm.

colonization sites for endophytic *Bacillus* strains, since for Gram-negative bacteria such as *Pseudomonas*, colonization was more evenly distributed and observed in older basal root parts or the root hair of barley (Buddrus-Schiemann *et al*., 2010). This might be linked to differences in chemoattractants and preferred metabolites associated with the different root regions and cell types, as has been indicated earlier (Brimecombe *et al*., 2007). However, the detailed mechanism of endophytic plant colonization by *B. mycoides* as well as a systematic comparison to tackle differences in the colonization mechanisms between Gram-negative and Gram-positive bacteria needs further thorough investigation.

Sequence analysis of in vivo *selected FPs optimized for* in planta *studies*

Early attempts to optimize the heterologous expression of GFP revealed that the fluorescence properties can be modulated by mutations within the fluorophore region, resulting in altered excitation and emission spectra (Ehrig *et al*., 1995). The S65T substitution leads, for instance, to GFP derivatives with a red-shifted excitation maximum and strongly increased fluorescence (Heim *et al*., 1995; Chiu *et al*., 1996). Since the wild-type GFP is prone to misfolding and aggregation, which causes reduced chromophore maturation and low yields, a variety of studies aimed at improving the folding properties of GFP and other FPs (Hsu *et al*., 2009). The FP variant Emerald contains the S65T and F64L mutations featured in enhanced GFP (eGFP), and has four additional point mutations that improve the efficiency of maturation and folding at 37°C, and increase the intrinsic brightness (Day and Davidson, 2009). Another approach to obtain improved FP variants is the adaptation of FP genes to the typical codon usage of the host organism, which in some

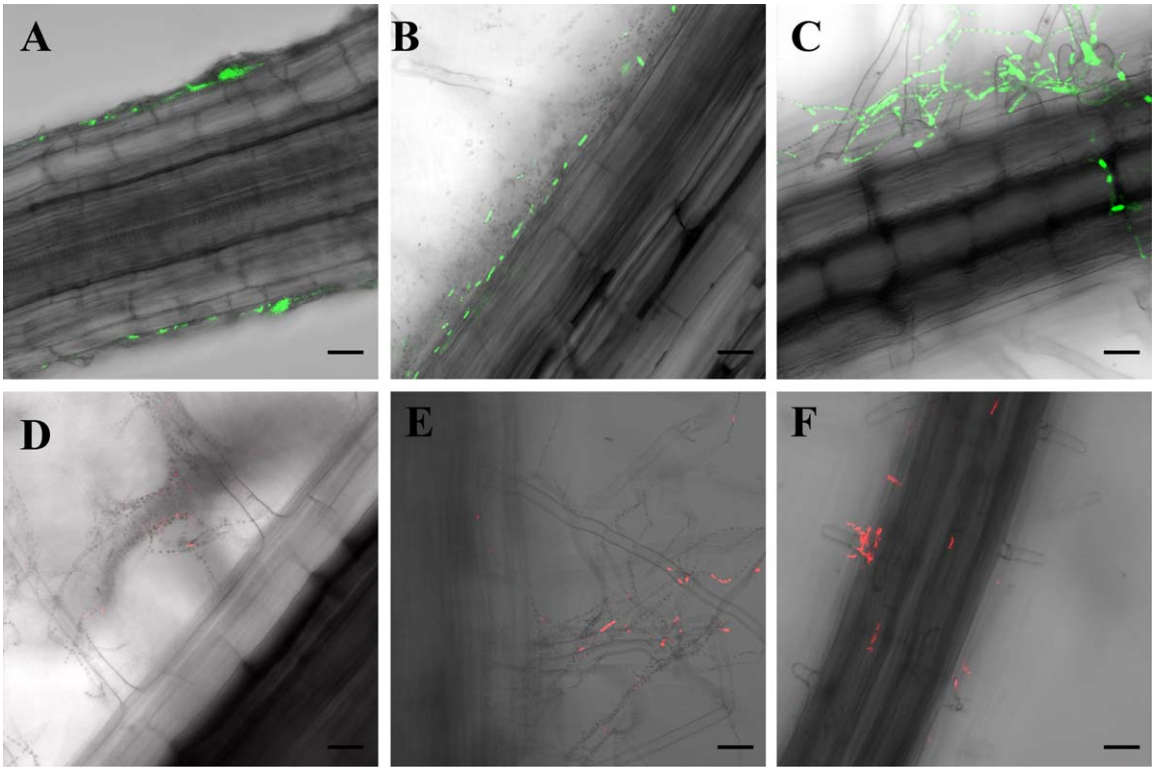

Fig. 7. *In planta* observation of life *B. mycoides* EC18 cells in the rhizosphere of Chinese cabbage. Labelling of *B. mycoides* with a set of *in vivo*-selected GFP and RFP variants allows *in situ* tracking of cabbage root colonization in a hydroponic system.
A. Epidermal colonization two DPI is visualized with the original sfGFP(Sp) reporter protein.
B. Cells labelled with the improved sfGFP(SPS6) variant aggregate on the root surface two DPI.
C. Cells labelled with the improved sfGFP(SPS6) interact with the root hair forming small microcolonies and establish endophytic colonization three DPI.
D. Tracking of *B. mycoides* cells labelled with the original mKate2 reporter is aggravated due to a low mKate2 brightness and high autofluorescence background of the plant tissue.
E. Detection of *B. mycoides* expressing the improved mKate2 (KPS12) reporter protein reveals the interaction of cells with root hairs two DPI and the entry into the endophytic colonization lifestyle three DPI (F). The scale bar represents 10 μm.

cases could improve the translation efficiency, resulting in higher FP expression and thus fluorescence signals (Sastalla *et al*., 2009; Leroch *et al*., 2011). Such codon optimized FPs have been developed for the cyan fluorescent protein and a yellow fluorescent protein in *B. anthracis* (Sastalla *et al*., 2009), for GFP and RFP in *Botrytis cinerea* (Leroch *et al*., 2011) and for GFP in *Zymoseptoria tritici* (Kilaru *et al*., 2015).

To analyse the changes associated with the improved functionality of the FP variants that were *in vivo* isolated from *B. mycoides*, the nucleotide mutations, amino acid exchanges as well as codon usage frequencies were compared between the mutated and the originating genes (Table 2). In comparison to the original sfGFP(Sp), the variant sfGFP(S618) carries the exchanges K156E and V176I. These two sites are solvent-exposed and located at the α-helix region between two β-strands (Supporting Information Fig. S4A). Pedelacq and colleagues (2006) reported that mutations at these flexible linker positions (e.g., Y145F and Y171V) are likely to eliminate aggregation-prone or off-pathway folded proteins from the folding trajectory. The variant sfGFP(S709) contains the three mutations T59I, P192P and Q204H; with the silent mutation P192P being distant from the chromophore, while the mutation T59I was close to the chromophore and buried in the centre of the ß-barrel (Supporting Information Fig. S4B). The mutation Q204H resides in the 10th ß-strand closely located to the chromophore. The ß-strand mutations F99S/M153T/V163A in GFPuv/cycle 3 variant were shown to change the surface hydrophobicity and, therefore, the aggregation propensity of the protein (Fukuda *et al*., 2000). The best performing GFP variant in this study, SPS6, contains the silent mutation A179A and a N39D exchange. The mutation Y39N was located between the 2nd and 3rd ß-strand (Supporting Information Fig. S4C) and was reported to increase folding rates and stability in sfGFP (Pedelacq *et al*., 2006). The substitution of asparagine to aspartic acid may further improve these effects.

Table 2. Overview of mutations of sfGFP(Sp) and mKate2 variants optimized for expression and *in planta* localization of *B. mycoides*.

FP variant	Nucleotide position[a]	Nucleotide exchange	Codon mutation	Amino acid position[a]	Amino acid mutation	Codon usage frequency of original amino acid[b]	Codon usage frequency of introduced amino acid[b]
S618	466	A→G	AAA→GAA	156	K156E	6.14	5.73
	526	G→A	GTT→ATT	176	V176I	3.12	5.17
S709	176	C→T	ACT→ATT	59	T59I	1.24	5.01
	576	A→G	CCA→CCG	192	P192P	1.64	0.76
	612	A→T	CAA→CAT	204	Q204H	3.03	1.63
SPS6	115	A→G	AAC→GAC	39	N39D	1.08	1.45
	537	T→C	GCT→GCC	179	A179A	2.98	1.21
K603	558	T→C	AAT→AAC	186	N186N	2.04	1.77
K713	455	G→A	GGT→GAT	152	G152D	1.12	3.07
KPS12	555	G→A	AAG→AAA	185	K185K	1.93	5.1
	616	G→T	GAT→TAT	206	D206Y	3.07	2.1
	660	T→G	CGT→CGG	220	R220R	0.69	0.99

a. Relative distance from translation start of FP.

b. According to codon usage frequency table for *B. mycoides* EC18 (accessible at the Genome 2D webserver http://server.molgenrug.nl/index.php).

The three *in vivo*-selected, optimized mKate2 mutants contained different nucleotide substitutions, which were either solely silent mutations [N186N in the case of mKate(K603)], solely amino acid exchanges [G152D in mKate(K713)] or a combination of both (K185K, R220R and D206Y in the brightest variant mKate(KPS12) obtained from pH shift experiments). The mutation sites are indicated on the 3D crystallographic structure of mKate2 in Supporting Information Fig. S4D–F. Since the RFPs are generally less well characterized than GFPs with regards to folding/unfolding kinetics and crystallization studies, the impact of these mutations on the improvement of fluorescence signal intensity and brightness or the folding and maturation efficacy is not readily explained. Although none of the mutations was located within the ß-barrel and in close proximity to the chromophore, some mutations may increase the performance by altering the aggregation behaviour or translation and folding speed by exchanging less preferred to more frequently used codons in *B. mycoides*. Especially the mutation K185K in the KPS12 variant increased the codon usage preference from 1.93% to 5.1% (Table 2). This might be associated with an increase of the translation and/or the folding speed, which probably prevents the accumulation of non-matured and non-functional protein precursors. Interestingly, the mKate2 variant FusionRed also had a mutation at this position (Shemiakina *et al*., 2012), which is reported to alter kinetics and efficiency of protein maturation.

Conclusion

By applying random mutagenesis and fluorescence-assisted cell sorting on sfGFP and mKate2 mutational libraries in life *B. mycoides* cells, we were able to isolate three brighter and well expressed variants of each FP protein for this bacterium. The improved performance of the FPs was confirmed at the population level by monitoring colony development on solid growth medium and at the single-cell level by FC and fluorescence microscopy of cells grown in liquid cultures. An extended applicability was proven by double-labelling of *B. mycoides* with the best performing variants sfGFP(SPS6) and mKate(KPS12). This revealed that i) the fluorescence signals were simultaneously detectable and clearly distinguishable from each other and ii) that chromosomal integration of the reporter proteins reduces cell-to-cell signal variations. To our knowledge, this is the first report of a successful dual-FP-labelling approach in bacilli of the *B. cereus sensu lato* group. Constitutive expression of the FPs from replicative plasmids did not affect the growth behaviour of *B. mycoides* and the plasmids were kept even without selection pressure by antibiotics over several cell generations. This indicates that FP expression does not represent a metabolic burden to the cells and altogether shows that the novel variants are suitable visualization markers without causing a loss of plant colonization ability. Finally, the optimized variants proved to be highly suitable for confocal laser scanning microscopy (CLSM) observations to study plant-microbe interactions and endophytic processes of *B. mycoides*. As a case study, we visualized the early stages of endophytic colonization in a hydroponic system. In line with previous studies, the formation of a multicellular matrix or microcolonies was revealed to be a prerequisite for endophytic colonization, in which the root hair and the elongation region of root hairs constitute potential entry sites to establish an endophytic lifestyle. The variants reported can be also used to study the expression of genes with weak promoters and

proved to be well expressed and detectable in additional soil- and rhizosphere-associated *Bacillus* species. Moreover, the brightest variant for both GFP and RFP were selected in the pH-shift group, which renders them especially suitable to study bacteria-plant interactions.

Experimental procedures

Strains and growth conditions

All strains, plasmids and primers used in this study are listed in Table 1. *B. mycoides* EC18 was isolated from the endosphere of a potato plant (Wijster, the Netherlands). *B. subtilis* HS3 and *B. amyloliquefaciens* HS9 were isolated from grass rhizosphere (Groningen, the Netherlands). The *Bacillus* strains were routinely cultured in Luria-Bertani (LB) medium at 30°C with aeration at 200 rpm. All *Escherichia coli* strains were cultured in LB broth at 37°C with aeration at 220 rpm. For cloning and selection purposes, ampicillin was added at a concentration of 100 μg/ml for *E. coli* and chloramphenicol and spectinomycin at a concentration of 4 μg/ml (LB-Cm4) and 100 μg/ml (LB-Spc100) for *Bacillus* strains respectively.

Random mutagenesis of fluorescent protein genes for E. coli *library construction*

E. coli libraries of randomly mutagenized sfGFP(Sp) or mKate2 proteins (Table 1) were generated with the GeneMorph II Random mutagenesis kit according to manufacturer's instructions (Agilent Technologies) as described elsewhere (Frenzel *et al*., 2017). In brief, the *sfgfp(Sp)* gene encoded on plasmid pKB01-sfGFP(Sp) was mutagenized by error-prone PCR using the primer pair pKBO1derMut_F and pKBO1derMut_R (Table 1). The XbaI/SphI digested PCR products were ligated into the equally cut replicative *Bacillus*/*E. coli*-shuttle plasmid pNW-Ppta-3TER (Table 1), which contains a *Parageobacillus thermoglucosidans*-derived constitutive promoter of the housekeeping *pta* gene and a threefold transcriptional terminator. In the same manner, the primer mKate2Mut_F and mKate2Mut_R (Table 1) were used to amplify and mutagenize *mKate2* from 0.1 ng of target DNA residing on plasmid pAD651 (Table 1). The XbaI/SphI cut fragments were cloned into the same restriction sites of the replicative *Bacillus-E. coli* shuttle vector pAD43-25 (Table 1), thereby releasing the *gfpmut3A* gene and placing *mKate2mut* expression under the control of the constitutive *upp* promoter from *B. cereus* UW85.

E. coli Top10 cells were transformed with the method as described by Sambrook *et al*. (Sambrook *et al*., 1989). From these, 20 randomly chosen colonies were grown separately in LB-Cm15 medium, and the mutation frequency of the FPs was estimated after plasmid isolation by double-stranded sequencing using the primer pairs pAD_for/pAD_rev for *mKate2* and pNW33N_for/pNW33N_rev for *sfgfp(Sp)* respectively (Table 1).

Whole plasmid libraries were generated as described previously (Frenzel *et al*., 2017). In brief, approximately 100 000 *E. coli* colonies were pooled after 24–30 h of growth at 37°C from plates by resuspension in LB medium and the vector mixture was extracted with the JETSTAR Plasmid Purification Kit according to the manufacturer's instruction (GENOMED, Löhne, Germany).

Preparation of competent B. mycoides *cells, electroporation and library setup*

B. mycoides EC18 aliquots were prepared for electroporation according to a protocol previously established for *B. cereus* (Ehling-Schulz *et al*., 2005). Library vector DNA was added in an amount of 1–2 μg to the cells, and electroporation was performed applying settings of 2.0 kV, 25 μF and 200 Ω in a 2-mm cuvette using a Bio Rad Gen Pulser II electroporation system (Bio-Rad). After addition of 1 ml LB medium, cells were grown for 2 h at 30°C and 150 rpm for recovery and then plated on LB-Cm4. After 16–24 h of growth at 30°C, colonies were harvested from the plates and pooled in LB medium. The libraries were stored at −80°C as 15% glycerol stocks.

Fluorescence-activated cell sorting of B. mycoides *FP libraries*

B. mycoides EC18 *sfGFP(Sp)mut* or *mKate2mut* libraries were inoculated in 50 ml of LB-Cm4 and grown at pH 7.0 or pH 6.0 to an OD_{600nm} of 0.3–0.6, representing the exponential phase of growth. Since *B. mycoides* shows extensive cell-chaining, a mild sonication step of 4 rounds of 3 × 10 pulses of 1s with an amplitude of 30% (Vibra Cell™, model VCX 130, Sonics and Materials, Newtown, CT, USA) was applied to disassemble the aggregated cells. Cells were sorted on a BD FACS Aria II (BD Biosciences) at 20 psi using a 70 μM nozzle at a flow rate of 1.0 with the highest sort precision mode (0–32-0 sort purity mask). Cellular debris and chained cells were excluded using a sequential gating strategy with FCS height versus widths, followed by SCC height versus width. For separation of the brightest variants, a cut-off of 3% of the brightest event in the first round of cell sorting and 0.3% of the brightest events in the second round of sorting with the light scatter parameters (ex: 488 nm, em: 525/50 nm, 505 LP filter for GFP; and ex: 592 nm, em 620/30 nm, 600 nm LP filter for RFP) was chosen. See Supporting Information Fig. S1 for a workflow scheme.

In total, 20000 cells were isolated by sorting and aliquots were plated on LB-Cm4 and grown 16–24 h at 30°C, while the remaining cells (ca. 10^4 CFU) were inoculated into fresh LB-Cm4 and grown either at the same pH (6.0 or 7.0) as the first cultures, or the pH was 'swapped' to sort bright variants functional at both pH 6.0 and pH 7.0. Cultures were incubated for 16 h at 30°C and 200 rpm until the following round of cell sorting.

Screening of FP variants and flow cytometry measurements

After FACS sorting, the final fluids containing bright cells were plated on LB-Cm4 plates and grown overnight at 30°C. The colonies were observed by Olympus MVX10 macro zoom fluorescence microscope equipped with a PreciseExcite light-emitting diode (LED) for fluorescence illumination. The filter setting for GFP was excitation at 460/480 nm and emission at 495/540 nm with a 485-nm dichromatic mirror; and for RFP the filter setting was excitation at 545/580 nm and emission at 610 nm with a 600 nm dichromatic mirror. Pictures were acquired with an Olympus XM10 monochrome camera (Olympus Corporation, Tokyo, Japan). Twenty of the brightest colonies in each screening group (pH 6.0, pH 7.0 or pH shift) were re-streaked and the fluorescence of individual cells was assessed by FC. The fluorescence of selected GFP variants was quantitatively determined with a FACSCanto flow cytometer (BD Biosciences) equipped with a 15 mW, 488 nm argon ion laser. All samples were grown in LB-Cm4 liquid medium, re-suspended in PBS and sonicated as described above to disperse cell-clumps prior to analysis. GFP emission was detected at 525/50 nm with an excitation of 488 nm. The RFP signals were measured in a FACS Aria II with excitation at 592 nm and emission at 620/30 nm. Per sample, 50 000 cells were analysed. Data acquisition and analysis was performed using the FACSDiva software (BD Biosciences) and the FCSalyzer software (version 0.9.13-alpha).

Electroporation of B. amyloliquefaciens*,* B. subtilis *and* B. cereus

For *B. amyloliquefaciens* and *B. subtilis*, one single colony was inoculated into 50 ml LBSP medium (LB supplemented with 0.5 M sorbitol and 50 mM KH_2PO_4 and K_2HPO_4) and grown to an OD_{600} of 0.65. Cells were collected by centrifugation at 5000 g, 4°C for 10 min. The supernatant was discarded and the pellet was washed with cold electroporation buffer (10% glycerol with 0.25 M sorbitol) for four times. Finally, the cells were suspended in 1 ml electroporation buffer. Aliquots of 100 μl were frozen in liquid nitrogen and stored at −80°C until the electroporation was performed. For *B. cereus*, electro-competent cells were prepared as described before (Ehling-Schulz *et al*., 2005). For all *Bacillus* strains, the electroporation was performed as described for *B. mycoides*.

Strain construction for double-FP-labelling of B. mycoides

The plasmid PYB was generated by replacing the pAMß1 replication origin (*ori*) of PATΔS28 (Namy *et al*., 1999) with a temperature sensitive *ori* from the PAW068 plasmid for Gram-positive bacteria (Wilson *et al*., 2007). Then a 1 kb-fragment of the α-amylase gene was amplified from the genome of *B. mycoides* EC18 with the primers amyF and amyR. This fragment was further digested with the KpnI and SacI enzymes and inserted into the PYB plasmid at the same restriction site to give rise to the plasmid PYB_amy. The *sfgfp*(SPS6) gene together with the P_{pta} promoter was inserted into PYB_amy at the restriction sites EcoRI and HindIII, which resulted in the plasmid PYB_amyGFP. This plasmid was then transformed into *B. mycoides* EC18 and plated on LB plates with 100 μg/ml spectinomycin. One colony was picked and grown in BHI liquid medium with100 μg/ml spectinomycin over night at 30°C. The culture was then diluted 100× with the same medium and grown at 37°C to block the replication of the plasmid. A serial dilution of the culture was plated on BHI-Spec100 agar and cultured at 37°C overnight. The colonies were checked by PCR for successful single cross-over recombination. The EC18 strain carrying the chromosomally integrated sfGFP(SPS6) reporter was used to make electrocompetent cells and the plasmid pAD-mKate(KPS12) was transformed into the strain. The double-labelled cells were selected on LB-Cm4/Spec100 agar grown at 30°C. Presence of the FP reporters was verified by double-stranded sequencing of the PCR products.

Strain construction for FP expression from mannose-inducible promoter

A fragment of the promoter P_{manP} that is positively regulated by mannose (Wenzel *et al*., 2011) was cloned from the plasmid pJOE8999 (Altenbuchner, 2016) using the primers PmanF and PmanR. The plasmid pAD-mKate(KPS12) was cleaved with EcoRI and XbaI, and the vector backbone was ligated with the P*manP* fragment cleaved by the same enzymes to give rise to pAD-KPS12-P*man*. To construct the mannose controlled GFP vector, the *gfp* (SPS6) gene was cut with XbaI and SphI from pNW-sfGFP(SPS6) and then inserted into pAD-KPS12-P*man* at the same restriction site to give the new plasmid pAD-SPS6-P*man*. The mannose-inducible FP strain was obtained by transforming the final plasmid

into the *B. mycoides* EC18 strain. The overnight culture of each strain was diluted 50 times with LB-CM4 with different concentrations of mannose. After around 6 hours of growth, fluorescence signals of the strains were measured by FC and images were captures with fluorescence microscopy.

Fluorescence microscopy

Single cell observation was performed with an Olympus IX71 microscope (Personal DV, Applied Precision; assembled by Imsol, Preston, UK) equipped with a Nomarski DIC and a 100 W mercury vapor lamp for FP excitation. A 10× eyepiece and a 100× phase-contrast objective were used to examine the cells. GFP variants were detected with excitation at 465–495 nm, 505 nm dichroic mirror and emission at 515–555 nm. RFP variants were detected with an excitation at 528–553 nm, 565 nm dichroic mirror and emission at 590–650 nm. Images were captured with a CoolSNAP HQ2 camera (Princeton Instruments, Trenton, NJ, USA). The intensity of single cell was calculated with the ImageJ software (https://imagej.nih.gov/ij/). The region of cells in which the fluorescence signal was quantified was selected manually. The total cell fluorescence was calculated by the following formula: corrected total cell fluorescence (CTCF) = Integrated Density – (Area of selected cell × Mean fluorescence of background readings) (Pozniak *et al*., 2016). At least 500 cells from three independent biological replicates were analysed.

Growth curves of FP-labelled B. mycoides *strains and plasmid stability assay*

B. mycoides strains transformed with the different FP variants were tested for their growth pattern and plasmid stability. The growth curve was determined by plotting the optical density values (OD_{600nm}) in LB liquid medium versus time. For the plasmid stability assay, each strain was grown to stationary phase in LB medium at 25°C (the same as plant culturing temperature) with 200 rpm aeration and then diluted by 50× in LB. The diluted culture was continued growing to stationary with the same conditions. Two more cycles of subsequent dilution were performed in the next two days. At day 3, the culture was serially diluted and plated on LB agar plates with or without chloramphenicol and the CFU/ml was calculated.

In situ *observation of FP labelled strains by confocal laser scanning microscopy*

Chinese cabbage seeds were surface sterilized in 70% ethanol for 2 min, followed by a bath in 3% sodium hypochlorite for 2 min. After the sterilization treatment, seeds were washed four times in sterile deionized water. The excessive water on the seeds surface was removed with autoclaved filter paper. The seeds were inoculated into Petri dishes containing 25% Hoagland solution (Hoagland and Arnon, 1950) solidified with 1% agar and incubated for germination and growth in a culture room at (25 ± 2°C) with a 12-h photoperiod for six days. The seedlings were then transferred to 3-L hydroponic trays containing 25% Hoagland's solution and continued to grow for 2 days. Hoagland solution was aerated using air stones connected to an aquarium air pump. The *B. mycoides* strains transformed with the different FP variants were grown to the exponential growth phase, and then 10 ml culture was collected and re-suspended in 25% Hoagland's solution. The hydroponic system was inoculated with a final concentration of 2×10^4 CFU/ml *B. mycoides* cells.

After 2–3 days of inoculation, the colonization of *B. mycoides* on the roots of the cabbage seedlings was assessed using a ZEISS LSM 800 CLSM (Carl Zeiss, Germany) equipped with diode lasers and GaAsP detector. Images for fluorescent light channels were taken simultaneously with images of the bright field channel. To achieve the maximum brightness of each FP and low background auto-fluorescence of the plant tissue, the settings of the confocal microscope were adjusted as follows: For GFP observation, 0.2% power of the 488 nm laser line was used for excitation and 509–546 nm was set as emission wavelength. For RFP detection, 1% power of the 561 nm laser line was used as excitation wavelength and 600–680 nm was set as emission wavelength. The pinhole size for GFP was 25 μm and for RFP was 30 μm, pixel scanning time was 2.06 μs and line scanning time was 2.47 ms with a line averaging of 2.

Acknowledgements

Conceived and designed experiments: EF, YY, OK. Performed the experiments: YY and EF. Performed isolation of *B. mycoides* and gave advice on plant cultures: JS, TME, JDvE. Wrote the manuscript: EF, YY, OK. All authors revised and approved the final manuscript. We thank Anne de Jong from the Molecular Genetics Department of the University of Groningen for programming the Gene Alignment Analysis Tool and Anita Kram from the Molecular Cell Biology department of the University of Groningen for her excellent technical advice on cell sorting. Y. Yi was supported by a grant of the Chinese Scholarship Council (CSC). The authors declare no competing financial interest.

References

Altenbuchner, J. (2016) Editing of the *Bacillus subtilis* genome by the CRISPR-Cas9 system. *Appl Environ Microbiol* **82**: 5421–5427.

Ambrosini, A., Stefanski, T., Lisboa, B.B., Beneduzi, A., Vargas, L.K., and Passaglia, L.M.P. (2016) Diazotrophic bacilli isolated from the sunflower rhizosphere and the potential of *Bacillus mycoides* B38V as biofertiliser. *Ann Appl Biol* **168**: 93–110.

Athukorala, S.N., Fernando, W.D., and Rashid, K.Y. (2009) Identification of antifungal antibiotics of *Bacillus* species isolated from different microhabitats using polymerase chain reaction and MALDI-TOF mass spectrometry. *Can J Microbiol* **55**: 1021–1032.

Barbez, E., Dünser, K., Gaidora, A., Lendl, T., and Busch, W. (2017) Auxin steers root cell expansion via apoplastic pH regulation in Arabidopsis thaliana. *Proc Natl Acad Sci USA* **114**: E4884–E4893.

Bargabus, R.L., Zidack, N., Sherwood, J., and Jacobsen, B. (2002) Characterisation of systemic resistance in sugar beet elicited by a non-pathogenic, phyllosphere-colonizing *Bacillus mycoides*, biological control agent. *Physiol Mol Plant Pathol* **61**: 289–298.

Bargabus, R.L., Zidack, N.K., Sherwood, J.E., and Jacobsen, B.J. (2004) Screening for the identification of potential biological control agents that induce systemic acquired resistance in sugar beet. *Biol Control* **30**: 342–350.

Bloemberg, G.V., Wijfjes, A.H., Lamers, G.E., Stuurman, N., and Lugtenberg, B.J. (2000) Simultaneous imaging of *Pseudomonas fluorescens* WCS365 populations expressing three different autofluorescent proteins in the rhizosphere: new perspectives for studying microbial communities. *Mol Plant Microbe Interact* **13**: 1170–1176.

Blossfeld, S., Gansert, D., Thiele, B., Kuhn, A.J., and Lösch, R. (2011) The dynamics of oxygen concentration, pH value, and organic acids in the rhizosphere of Juncus spp. *Soil Biol Biochem* **43**: 1186–1197.

Buddrus-Schiemann, K., Schmid, M., Schreiner, K., Welzl, G., and Hartmann, A. (2010) Root colonization by *Pseudomonas* sp. DSMZ 13134 and impact on the indigenous rhizosphere bacterial community of barley. *Microb Ecol* **60**: 381–393.

Brimecombe, M.J., De Leij, F.A.A.M., Lynch, J.M. (2007) Rhizodeposition and Microbial Populations. *In The Rhizosphere- Biochemistry and Organic Substances at the Soil-Plant Interface*. Pinton, R., Varanini, Z., Nannipieri, P. (eds). Baco Raton, FL: CRC Press,. pp. 73–89.

Chiu, W., Niwa, Y., Zeng, W., Hirano, T., Kobayashi, H., and Sheen, J. (1996) Engineered GFP as a vital reporter in plants. *Curr Biol* **6**: 325–330.

Chudakov, D.M., Matz, M.V., Lukyanov, S., and Lukyanov, K.A. (2010) Fluorescent proteins and their applications in imaging living cells and tissues. *Physiol Rev* **90**: 1103–1163.

Craggs, T.D. (2009) Green fluorescent protein: structure, folding and chromophore maturation. *Chem Soc Rev* **38**: 2865–2875.

Das, A.K., Hasegawa, J.Y., Miyahara, T., Ehara, M., and Nakatsuji, H. (2003) Electronic excitations of the green fluorescent protein chromophore in its protonation states: SAC/SAC-CI study. *J Comput Chem* **24**: 1421–1431.

Day, R.N., and Davidson, M.W. (2009) The fluorescent protein palette: tools for cellular imaging. *Chem Soc Rev* **38**: 2887–2921.

Di Franco, C., Pisaneschi, G., and Beccari, E. (2000) Molecular analysis of two rolling-circle replicating cryptic plasmids, pBMYdx and pBMY1, from the soil gram-positive *Bacillus mycoides*. *Plasmid* **44**: 280–284.

Di Franco, C., Beccari, E., Santini, T., Pisaneschi, G., and Tecce, G. (2002) Colony shape as a genetic trait in the pattern-forming *Bacillus mycoides*. *BMC Microbiol* **2**: 33.

Dunn, A.K., and Handelsman, J. (1999) A vector for promoter trapping in *Bacillus cereus*. *Gene* **226**: 297–305.

Ehling-Schulz, M., Vukov, N., Schulz, A., Shaheen, R., Andersson, M., Martlbauer, E., and Scherer, S. (2005) Identification and partial characterization of the nonribosomal peptide synthetase gene responsible for cereulide production in emetic *Bacillus cereus*. *Appl Environ Microbiol* **71**: 105–113.

Ehrig, T., O'Kane, D.J., and Prendergast, F.G. (1995) Green-fluorescent protein mutants with altered fluorescence excitation spectra. *FEBS Lett* **367**: 163–166.

Eijlander, R.T., and Kuipers, O.P. (2013) Live-cell imaging tool optimization to study gene expression levels and dynamics in single cells of *Bacillus cereus*. *Appl Environ Microbiol* **79**: 5643–5651.

Fan, B., Chen, X.H., Budiharjo, A., Bleiss, W., Vater, J., and Borriss, R. (2011) Efficient colonization of plant roots by the plant growth promoting bacterium Bacillus amyloliquefaciens FZB42, engineered to express green fluorescent protein. *J Biotechnol* **151**: 303–311.

Frenzel, E., Legebeke, J., van Strahlen, A., van Kranenburg, R., Kuipers, O.P. (2017) *In vivo* selection of sfGFP variants with improved and reliable functionality in industrially important thermophilic bacteria. Biotechnol Biofuels. (in press).

Fukuda, H., Arai, M., and Kuwajima, K. (2000) Folding of green fluorescent protein and the cycle3 mutant. *Biochemistry* **39**: 12025–12032.

Germaine, K., Keogh, E., Garcia-Cabellos, G., Borremans, B., Lelie, D., Barac, T., *et al*. (2004) Colonisation of poplar trees by gfp expressing bacterial endophytes. *FEMS Microbiol Ecol* **48**: 109–118.

Guetsky, R., Shtienberg, D., Elad, Y., Fischer, E., and Dinoor, A. (2002) Improving biological control by combining biocontrol agents each with several mechanisms of disease suppression. *Phytopathology* **92**: 976–985.

Guinebretière, M.-H., Thompson, F.L., Sorokin, A., Normand, P., Dawyndt, P., Ehling-Schulz, M., *et al*. (2008) Ecological diversification in the *Bacillus cereus* Group. *Environ Microbiol* **10**: 851–865.

Hebisch, E., Knebel, J., Landsberg, J., Frey, E., Leisner, M., and Hofmann, A. (2013) High variation of fluorescence protein maturation times in closely related *Escherichia coli* strains. *PLoS One* **8**: e75991.

Heim, R., Prasher, D.C., and Tsien, R.Y. (1994) Wavelength mutations and posttranslational autoxidation of green fluorescent protein. *Proc Natl Acad Sci USA* **91**: 12501–12504.

Heim, R., Cubitt, A.B., and Tsien, R.Y. (1995) Improved green fluorescence. *Nature* **373**: 663–664.

Hoagland, D.R., and Arnon, D.I. (1950) The water-culture method for growing plants without soil. *Circular California Agric Exp Station* **C347**: 36–39.

Hsu, S.T., Blaser, G., and Jackson, S.E. (2009) The folding, stability and conformational dynamics of beta-barrel fluorescent proteins. *Chem Soc Rev* **38**: 2951–2965.

Ji, X., Lu, G., Gai, Y., Zheng, C., and Mu, Z. (2008) Biological control against bacterial wilt and colonization of mulberry by an endophytic *Bacillus subtilis* strain. *FEMS Microbiol Ecol* **65**: 565–573.

Kilaru, S., Schuster, M., Studholme, D., Soanes, D., Lin, C., Talbot, N.J., and Steinberg, G. (2015) A codon-optimized green fluorescent protein for live cell imaging in *Zymoseptoria tritici*. *Fungal Genet Biol* **79**: 125–131.

Kjos, M., Aprianto, R., Fernandes, V.E., Andrew, P.W., van Strijp, J.A.G., Nijland, R., *et al*. (2015) Bright fluorescent Streptococcus pneumoniae for live-cell imaging of host-pathogen interactions. *J Bacteriol* **197**: 807–818.

Kloepper, J.W., Ryu, C.-M., and Zhang, S. (2004) Induced systemic resistance and promotion of plant growth by *Bacillus* spp. *Phytopathology* **94**: 1259–1266.

Kremers, G.-J., Gilbert, S.G., Cranfill, P.J., Davidson, M.W., and Piston, D.W. (2011) Fluorescent proteins at a glance. *J Cell Sci* **124**: 157–160.

Larrainzar, E., O'gara, F., and Morrissey, J.P. (2005) Applications of autofluorescent proteins for in situ studies in microbial ecology. *Annu Rev Microbiol* **59**: 257–277.

Leroch, M., Mernke, D., Koppenhoefer, D., Schneider, P., Mosbach, A., Doehlemann, G., and Hahn, M. (2011) Living colors in the gray mold pathogen *Botrytis cinerea*: codon-optimized genes encoding green fluorescent protein and mCherry, which exhibit bright fluorescence. *Appl Environ Microbiol* **77**: 2887–2897.

Nakamura, L., and Jackson, M. (1995) Clarification of the taxonomy of *Bacillus mycoides*. *Int J Syst Evol Microbiol* **45**: 46–49.

Namy, O., Mock, M., and Fouet, A. (1999) Co-existence of *clpB* and *clpC* in the Bacillaceae. *FEMS Microbiol Lett* **173**: 297–302.

Neher, O.T., Johnston, M.R., Zidack, N.K., and Jacobsen, B.J. (2009) Evaluation of *Bacillus mycoides* isolate BmJ and *B. mojavensis* isolate 203-7 for the control of anthracnose of cucurbits caused by *Glomerella cingulata* var. orbiculare. *Biol Control* **48**: 140–146.

Overkamp, W., Beilharz, K., Detert Oude Weme, R., Solopova, A., Karsens, H., Kovacs, A.T., *et al*. (2013) Benchmarking various green fluorescent protein variants in *Bacillus subtilis*, *Streptococcus pneumoniae*, and *Lactococcus lactis* for Live Cell Imaging. *Appl Environ Microbiol* **79**: 6481–6490.

Pedelacq, J.D., Cabantous, S., Tran, T., Terwilliger, T.C., and Waldo, G.S. (2006) Engineering and characterization of a superfolder green fluorescent protein. *Nat Biotechnol* **24**: 79–88.

Piatkevich, K.D., Hulit, J., Subach, O.M., Wu, B., Abdulla, A., Segall, J.E., and Verkhusha, V.V. (2010) Monomeric red fluorescent proteins with a large Stokes shift. *Proc Natl Acad Sci USA* **107**: 5369–5374.

Pozniak, P.D., Darbinyan, A., and Khalili, K. (2016) TNF-α/TNFR2 regulatory axis stimulates EphB2-mediated neuroregeneration via activation of NF-κB. *J Cell Physiol* **231**: 1237–1248.

Prasher, D.C., Eckenrode, V.K., Ward, W.W., Prendergast, F.G., and Cormier, M.J. (1992) Primary structure of the *Aequorea victoria* green-fluorescent protein. *Gene* **111**: 229–233.

Prieto, P., Schiliro, E., Maldonado-Gonzalez, M.M., Valderrama, R., Barroso-Albarracin, J.B., and Mercado-Blanco, J. (2011) Root hairs play a key role in the endophytic colonization of olive roots by *Pseudomonas* spp. with biocontrol activity. *Microb Ecol* **62**: 435–445.

Rasko, D.A., Ravel, J., Økstad, O.A., Helgason, E., Cer, R.Z., Jiang, L., *et al*. (2004) The genome sequence of Bacillus cereus ATCC 10987 reveals metabolic adaptations and a large plasmid related to Bacillus anthracis pXO1. *Nucleic Acids Res* **32**: 977–988.

Rizzo, M.A., Davidson, M.W., and Piston, D.W. (2009) Fluorescent protein tracking and detection: fluorescent protein structure and color variants. *Cold Spring Harb Protoc* **2009**: pdb.top63.

Rodriguez, E.A., Tran, G.N., Gross, L.A., Crisp, J.L., Shu, X., Lin, J.Y., and Tsien, R.Y. (2016) A far-red fluorescent protein evolved from a cyanobacterial phycobiliprotein. *Nat Methods* **13**: 763–769.

Samapundo, S., Devlieghere, F., Xhaferi, R., and Heyndrickx, M. (2014) Incidence, diversity and characteristics of spores of psychrotolerant spore formers in various REPFEDS produced in Belgium. *Food Microbiol* **44**: 288–295.

Sambrook, J., Fritsch, E.F., and Maniatis, T. (1989) *Molecular Cloning: A Laboratory Manual*. New York: Cold Spring Harbor Laboratory Press.

Sastalla, I., Chim, K., Cheung, G.Y., Pomerantsev, A.P., and Leppla, S.H. (2009) Codon-optimized fluorescent proteins designed for expression in low-GC gram-positive bacteria. *Appl Environ Microbiol* **75**: 2099–2110.

Shaner, N.C., Steinbach, P.A., and Tsien, R.Y. (2005) A guide to choosing fluorescent proteins. *Nat Methods* **2**: 905–909.

Shapiro, J.A. (1998) Thinking about bacterial populations as multicellular organisms. *Annu Rev Microbiol* **52**: 81–104.

Shemiakina, I.I., Ermakova, G.V., Cranfill, P.J., Baird, M.A., Evans, R.A., Souslova, E.A., *et al*. (2012) A monomeric red fluorescent protein with low cytotoxicity. *Nat Commun* **3**: 1204.

Shimomura, O., Johnson, F.H., and Saiga, Y. (1962) Extraction, purification and properties of aequorin, a bioluminescent protein from the luminous hydromedusan, *Aequorea*. *J Cell Physiol* **59**: 223–239.

Shu, X., Shaner, N.C., Yarbrough, C.A., Tsien, R.Y., and Remington, S.J. (2006) Novel chromophores and buried charges control color in mFruits. *Biochemistry* **45**: 9639–9647.

Stefan, M., Munteanu, N., Stoleru, V., Mihasan, M., and Hritcu, L. (2013) Seed inoculation with plant growth promoting rhizobacteria enhances photosynthesis and yield of runner bean (*Phaseolus coccineus* L.). *Sci Hortic* **151**: 22–29.

Turchi, L., Santini, T., Beccari, E., and Di Franco, C. (2012) Localization of new peptidoglycan at poles in *Bacillus mycoides*, a member of the *Bacillus cereus* group. *Arch Microbiol* **194**: 887–892.

Wenzel, M., Müller, A., Siemann-Herzberg, M., and Altenbuchner, J. (2011) Self-inducible *Bacillus subtilis* expression system for reliable and inexpensive protein production by high-cell-density fermentation. *Appl Environ Microbiol* **77**: 6419–6425.

Wilson, A.C., Perego, M., and Hoch, J.A. (2007) New transposon delivery plasmids for insertional mutagenesis in *Bacillus anthracis*. *J Microbiol Methods* **71**: 332–335.

Yi, Y., de Jong, A., Frenzel, E., and Kuipers, O.P. (2017) Comparative transcriptomics of *Bacillus mycoides* strains in response to potato-root exudates reveals different genetic adaptation of endophytic and soil isolates. *Front Microbiol* **8**: 1487.

Supporting Information

Additional Supporting Information may be found in the online version of this article at the publisher's web-site:

Fig. S1. Workflow for *in vivo* isolation of optimized GFP [sfGFP(Sp)] and RFP (mKate2) variants from *B. mycoides*. GFP and RFP mutant libraries were constructed by random mutagenesis and cloned into the *E. coli-Bacillus* shuttle plasmids pNW-Ppta-3TER and pAD43-25 respectively. After transformation of *B. mycoides*, cells were grown in different pH conditions and two rounds of fluorescence-activated cell sorting were performed with a subsequent enrichment of $\sim$ 3% and $\sim$ 0.3% of the brightest single cells from the total population. After plating, colonies displaying the highest fluorescence signals were selected by use of a fluorescence stereo microscope.

Fig. S2. Analysis of metabolic burden of FP expression and plasmid stability in *B. mycoides* EC18. (A) OD 600 measurements in LB medium comparing the growth behaviour of wild-type EC 18 and its derivative strains carrying the reporter proteins on replicative plasmids. (B) Cultivation of subsequent culture dilutions and final plating assay to determine the plasmid presence with and without antibiotic pressure in *B. mycoides*. For details, see *Experimental Procedures*.

Fig. S3. Comparison of the performance of original and optimized FP variants fused to a weak, mannose-inducible promoter. (A) Detection of the expression of sfGFP(Sp) and the optimized sfGFP(SPS6) protein in exponential phase cells of *B. mycoides* EC18 by FC (B): Detection of the expression of mKate2 and optimized mKate(KPS12) in exponential phase cells of *B. mycoides* EC18 by FC.

Fig. S4. Three-dimensional structure of sfGFP(Sp) (PDB ID: 2B3P) and mKate2 (PDB ID: 3BXB) variants. The mutation sites of the improved FP variants are indicated in yellow. The chromophore was highlighted in green for sfGFP (A–C) and red for mKate2 (D–F). A: S618; B: S709; C: SPS6; D: K603; E: K713; F: KPS12. The structure was visualized with the Cn3D software.